

**Decohesion Elements using Two and
Three-Parameter Mixed-Mode Criteria**

Carlos G. Dávila

NASA Langley Research Center
Hampton, VA

Pedro P. Camanho

University of Porto, Portugal

American Helicopter Society Conference

Williamsburg, VA

October 29-November 1, 2001

Decohesion Elements using Two and Three-Parameter Mixed-Mode Criteria

Carlos G. Dávila

NASA Langley Research Center, Hampton, VA 23681

Pedro P. Camanho

University of Porto, Portugal

Abstract

An 8-node decohesion element implementing different criteria to predict delamination growth under mixed-mode loading is proposed. The element is used at the interface between solid finite elements to model the initiation and propagation of delamination. A single displacement-based damage parameter is used in a softening law to track the damage state of the interface. The power law criterion and a three-parameter mixed-mode criterion are used to predict delamination growth. The accuracy of the predictions is evaluated in single mode delamination and in the mixed-mode bending tests.

Introduction

Delamination is one of the predominant forms of failure in laminated composites due to the lack of reinforcement in the thickness direction. Delamination as a result of impact or a manufacturing defect can cause a significant reduction in the compressive load-carrying capacity of a structure. The stress gradients that occur near geometric discontinuities such as ply drop-offs, stiffener terminations and flanges (Figure 1), bonded and bolted joints, and access holes promote delamination initiation, trigger intraply damage mechanisms, and cause a significant loss of structural integrity.

The fracture process of high performance composite laminates is quite complex, involving not only interlaminar damage (delamination), but also intralaminar damage mechanisms (e.g. matrix cracking, fiber fracture).

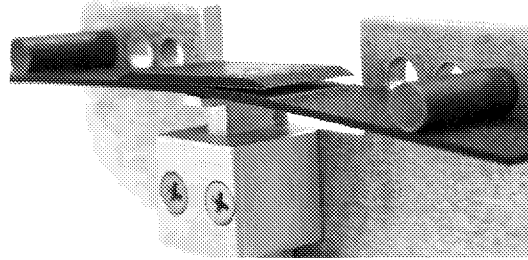


Figure 1. Experiment illustrating stiffener-flange debonding.

The objective of this paper is to present a method to simulate progressive delamination with decohesion elements based on a new mixed-mode failure criterion. The numerical predictions are compared with analytical closed-form solutions and experimental results.

Numerical Simulation of Delamination

The study of delamination mechanics may be divided into the study of delamination initiation and the analysis of delamination propagation. Delamination initiation analyses are usually based on stresses and use criteria such as the quadratic interaction of the interlaminar stresses in conjunction with a characteristic distance^{1, 2}. The characteristic distance is an averaging length that is a function of geometry and material properties, so its determination always requires extensive testing.

Most analyses of delamination growth apply a fracture mechanics approach and evaluate strain energy release rates G for self-similar delamination growth. The G values are usually evaluated using the virtual crack closure technique (VCCT) proposed by Rybicki and Kanninen³. The VCCT technique is based on Irwin's assumption that when a crack extends by a small amount, the energy released in the process is equal to the work required to close the crack to its original length. The Mode I, Mode II, and Mode III energy release rates can then be computed from the nodal forces and displacements obtained from the solution of a finite element model. The approach is computationally effective since the energy release rates can be obtained from only one analysis.

In the present paper, an approach is proposed that is well suited to nonlinear progressive failure analyses where both ply damage and delaminations are present. The approach consists of placing interfacial decohesion elements between composite layers. A decohesion failure criterion that combines aspects of strength-based analysis and Fracture Mechanics is used to simulate debonding by softening the element. The proposed constitutive equations for the interface are phenomenological mechanical relations between the tractions and interfacial separations. With increasing interfacial separation, the tractions across the interface reach a maximum, decrease, and vanish when complete decohesion occurs. The work of normal and tangential separation can be related to the critical values of energy release rates⁴.

Decohesion can be implemented as a material response such as the Dugdale-Barenblatt (D-B) type cohesive zone⁵. The D-B cohesive zone model was first applied to the analysis of concrete cracking by Hillerborg et al⁶. The concept has also been used by Needleman⁷ to simulate fast crack growth in brittle solids. Needleman considered that cohesive zone models are particularly attractive when interfacial strengths are relatively weak when compared with the adjoining material, as is the case in composite laminates.

In order to predict the initiation and growth of delaminations, an 8-node decohesion element shown in Fig. 2 was developed and implemented in the ABAQUS finite element code. The development of this element is based on prior work^{8,9}. The decohesion element is used to model the interface between sublaminates or between two bonded components. The element consists of a zero-thickness volumetric element in which the interpolating shape functions for the top and bottom faces are compatible with the kinematics of the elements that are being connected to it. The material response built into the element represents damage using a cohesive zone ahead of crack tip to predict delamination growth. The concept of interface elements has been used in different types of problems: compression after impact^{10,11}, damage growth from discontinuous plies¹², and diametrical compression of composite cylinders¹³.

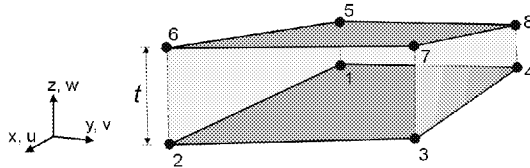


Figure 2. Eight-node decohesion element; $t=0$.

Constitutive Equations

The need for an appropriate constitutive equation in the formulation of the interface element is fundamental for

an accurate simulation of the interlaminar cracking process. A constitutive equation is used to relate the traction σ to the relative displacement δ at the interface. Some softening models that have been proposed are shown in Fig. 3 and include: linear elastic-perfectly plastic; linear elastic-linear softening; linear elastic-progressive softening; linear elastic-regressive softening; and Needleman⁷. One characteristic of all softening models is that the cohesive zone can still transfer load after the onset of damage (δ^o in Figure 3). For pure Mode I, II or III loading, after the interfacial normal or shear stresses attain their respective interlaminar tensile or shear strengths, the stiffnesses are gradually reduced to zero. The area under the stress-relative displacement curves is the respective (Mode I, II or III) fracture energy. Using the definition of the J integral proposed by Rice¹⁴, it can be shown that for small cohesive zones,

$$\int_0^{\delta^F} \sigma(\delta) d\delta = G_c \quad (1)$$

where G_c is the critical energy release rate for a particular mode, and δ^F is the corresponding relative displacement at failure (δ_{pp} , δ_{pro} , δ_{lin} , δ_{Ne} , or δ_{re} in Figure 3).

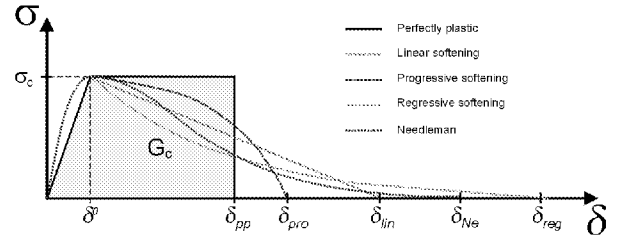


Figure 3. Strain softening constitutive models.

Bilinear Softening Model

The linear elastic-linear softening (bilinear) model is the simplest to implement, and is most commonly used^{10,11,15-17}. The double cantilever beam test shown in Figure 4 illustrates the material response. Point 1 in Figure 4 is subjected to a low tensile load that is within the linear elastic range. A high initial stiffness K_p (penalty) holds the top and bottom faces of the interface element together. Point 2 represents the onset of damage. In single-mode delamination, the traction at point 2 is equal to the corresponding interlaminar strength of the material, σ_c . As the relative displacement increases, the interface accumulates damage and the traction is lower than the strength (point 3). The energy released at point 3 is the area of the triangle 0-2-3. If the load were to reverse, point 3 would unload to the origin, as shown in the figure.

The critical value of the energy release rate is attained at point 4. For any relative displacement larger than point 4,

the interface does not carry any tensile or shear loads (point 5). In other words, at point 4 all the available interfacial fracture energy has been completely consumed. Note that when modeling delamination with a softening response, the delamination tip is not defined explicitly. While the onset of damage occurs at point 2 in Figure 4, the delamination tip could be defined as the point where the tractions at the interface are zero, which is point 4.

The softening response illustrated in Figure 4 is representative of the tension or the shear response but not compression. It is assumed that compression loads do not cause delamination or softening, and the effect of compression on damage of the interface was neglected in the present work.

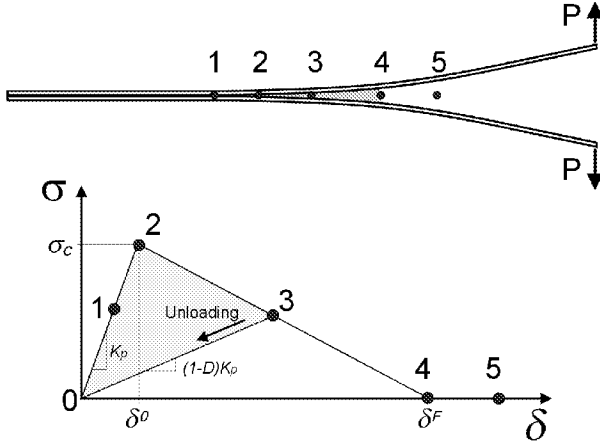


Figure 4. Bilinear constitutive model.

The problem of contact of the crack faces after failure is addressed by re-applying the normal penalty stiffness. The process of reapplying the normal stiffness when interpenetration is detected is typical of solution procedures of contact problems using penalty methods in a constrained variational formulation.

The concept of decohesion zones to simulate delamination growth in composites is usually implemented by means of interface elements connecting the individual plies of a composite laminate. Decohesion elements can model the discontinuity introduced by the growth of delaminations. They can be divided into two main groups: continuous interface elements and point interface elements. Several types of continuous interface elements have been proposed, ranging from plane interface elements with zero thickness connecting solid elements^{10, 11}; plane interface elements with finite thickness connecting shell elements¹³; line interface elements^{12, 17, 18}; and spring interface elements that connect pairs of nodes^{15, 16}.

The bilinear interfacial constitutive response shown in Figure 4 can be implemented as follows:

i) $\delta < \delta^0 \Rightarrow$ the constitutive equation is given by:

$$\sigma = K_p \delta \quad (2)$$

ii) $\delta^0 \leq \delta < \delta^F \Rightarrow$ the constitutive equation is given by:

$$\sigma = (1-D)K_p \delta \quad (3)$$

where D represents the damage accumulated at the interface, which is zero initially, and reaches 1 when the material is fully damaged.

iii) $\delta \geq \delta^F \Rightarrow$ all the penalty stiffnesses are set equal to zero. If crack closure is detected, interpenetration is prevented by reapplying only the normal stiffness. Frictional effects are neglected.

The properties required to define the bilinear interfacial softening behavior are the initial stiffness (penalty) K_p , the fracture energies G_{IC} , G_{IIC} , and G_{IIIC} and the corresponding nominal interlaminar tensile and shear strengths, T and S . The accuracy of the analysis depends on the penalty stiffness K_p that is chosen. High values of K_p avoid interpenetration of the crack faces but can lead to numerical problems. Several values have been proposed for the penalty stiffness, K_p : 10^7 N/mm³ [Ref. 10], 5.7×10^7 N/mm³ [Ref. 19], 10^8 N/mm³ [Ref. 16]. Other authors have determined the value for the penalty stiffness as a function of the interface properties. Daudeville et al.²⁰ have modeled the interface as a resin rich zone of small thickness, t_i , and proposed a penalty stiffnesses defined as:

$$K_p^I = \frac{E_3}{t_i}; K_p^{II} = \frac{2G_{13}}{t_i}; K_p^{III} = \frac{2G_{23}}{t_i} \quad (4)$$

where G_{23} , G_{13} , and E_3 are the elastic moduli of the resin rich zone. After a substantial number of numerical experiments, Moura²¹ determined that a penalty stiffnesses of only 10^6 N/mm³ for all modes produces essentially the same results while avoiding potential convergence problems during the nonlinear procedure.

In order to fully define the interfacial behavior, the unloading response must be specified. Petrossian et al.¹⁶ have proposed an unloading curve with a slope corresponding to Hooke's law. Such a procedure, typically used in the formulation of plasticity problems, would lead to the use of the same penalty stiffness when reloading and to permanent relative displacements along the interface when the load reverts to zero. Crisfield et al.^{17, 18} and Daudeville²⁰, on the other hand, have proposed that with reversing strains the material unloads directly toward the origin, as shown in Figure 4. The assumption is that during reloading the interfacial stiffness is lower than the original (undamaged) stiffness. Such a procedure simulates the effects of the previous damage mechanisms that occurred along the interface and was therefore adopted in the present work.

Mixed Mode Delamination Criterion

In structural applications of composites, delamination growth is likely to occur under mixed-mode loading. Therefore, a general formulation for interface elements must deal with mixed-mode delamination growth problems.

Under pure Mode I, II or III loading, the onset of damage at the interface can be determined simply by comparing the stress components with their respective allowables. Note that the onset of damage does not imply the initiation of delamination, since the tractions closing the crack at onset are at their maximum value. Under mixed-mode loading, however, damage onset may occur before any of the stress components involved reach their respective allowables.

A mixed-mode criterion is proposed here that is based on a few simplifying assumptions. Firstly, it is assumed that delamination initiation can be predicted using the quadratic failure criterion

$$\sqrt{\left(\frac{\sigma_z}{T}\right)^2 + \left(\frac{\tau_{xz}}{S}\right)^2 + \left(\frac{\tau_{yz}}{S}\right)^2} = 1 \quad \text{for } \sigma_z > 0 \quad (5)$$

$$\sqrt{\left(\frac{\tau_{xz}}{S}\right)^2 + \left(\frac{\tau_{yz}}{S}\right)^2} = 1 \quad \text{for } \sigma_z \leq 0 \quad (6)$$

where σ_z is the transverse normal traction and τ_{xz} and τ_{yz} are the transverse tractions. T and S are the nominal normal tensile and shear strengths, respectively.

The delamination mechanisms in Mode II and Mode III are assumed to be the same. Therefore, Mode III can be combined with Mode II by using a total tangential displacement δ_{II} defined as the norm of the two orthogonal tangential relative displacements δ_x and δ_y as

$$\delta_{II} = \sqrt{\delta_x^2 + \delta_y^2} \quad (7)$$

The total mixed-mode relative displacement δ_m is defined as

$$\delta_m = \sqrt{\delta_z^2 + \delta_{II}^2} \quad (8)$$

where δ_z is the relative opening (Mode I) displacement. Using the same penalty stiffness in Modes I and II, the tractions are

$$\begin{aligned} \sigma_z &= K_P \delta_z \\ \tau_{xz} &= K_P \delta_x \\ \tau_{yz} &= K_P \delta_y \end{aligned} \quad (9)$$

The single-mode failure initiation displacements are then

$$\begin{aligned} \delta_I^0 &= T / K_P \\ \delta_{II}^0 &= S / K_P \end{aligned} \quad (10)$$

where T and S are the nominal tensile and shear strengths of the interface. If the relative opening displacement δ_z is not zero, the mode mixity can be expressed by

$$\beta = \frac{\delta_{II}}{\delta_z} \quad (11)$$

The mixed-mode damage initiation displacement is obtained by substituting Eqs. 7-11 into 5, which gives:

$$\delta^0 = \delta_I^0 \delta_{II}^0 \sqrt{\frac{1 + \beta^2}{(\delta_{II}^0)^2 + (\beta \delta_I^0)^2}} \quad (12)$$

The criteria used to predict delamination propagation under mixed-mode loading conditions are generally established in terms of the energy release rates and fracture toughness. The most widely used criteria to predict the interaction of the energy release rates in mixed mode is the power law given by the expression:

$$\left(\frac{G_I}{G_{IC}}\right)^\alpha + \left(\frac{G_{II}}{G_{IIC}}\right)^\alpha = 1 \quad (13)$$

The exponent α in the power law is usually selected to be either 1 or 2, in which case the criterion is a two-parameter interaction law with parameters G_{IC} and G_{IIC} .

Reeder²² performed mixed-mode bending (MMB) tests to measure the mixed-mode I and II interlaminar fracture toughness of composites, providing valuable experimental data to assess criteria that have been proposed to predict delamination growth. The linear criterion obtained with $\alpha=1$ in Eq. 13 was found to be suitable for thermoplastic PEEK matrix composites, its results being comparable to more complex interaction functions. However, both the linear and quadratic interaction criteria failed to capture adequately the dependence of the mixed-mode fracture toughness on the mode ratio in epoxy composites.

In order to accurately account for the variation of fracture toughness as a function of mode ratio, a recently proposed three-parameter criterion (B-K criterion, Ref. 23) is implemented here. The B-K criterion is established in terms of the single mode fracture toughnesses G_{IC} and G_{IIC} and a parameter η :

$$G_T = G_{IC} + (G_{IIC} - G_{IC}) \left(\frac{G_{II}}{G_T}\right)^\eta \quad (14)$$

Reeder²⁴ applied the B-K criterion to mixed mode test results of IM7/977-2 and obtained a best fit using $\eta=1.45$, which is shown in Figure 5. The linear ($\alpha=1$) and quadratic ($\alpha=2$) criteria, which are also shown in Figure 5, do not correlate well with the experimental results for this material.

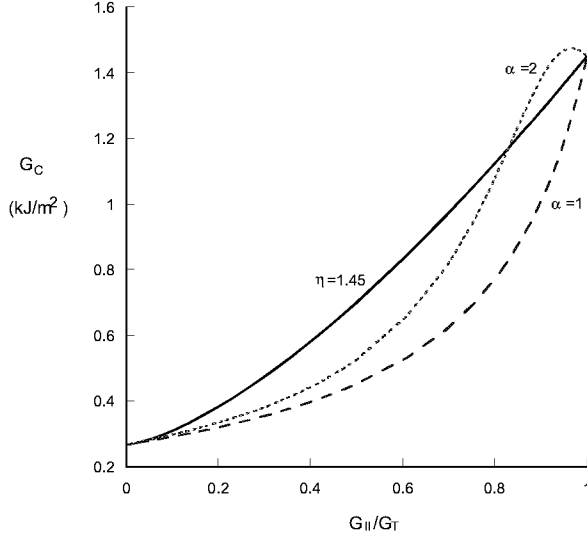


Figure 5. G_C versus G_{II}/G_I mode ratio for IM7/99-2.

For the bilinear stress-displacement softening law assumed here, the critical energy release rates in Mode I and Mode II are simply the areas under the triangle 0-2-4 in Figure 4.

$$G_{Ic} = \frac{T \delta_I^F}{2} \quad ; \quad G_{IIc} = \frac{S \delta_{II}^F}{2} \quad (15)$$

where δ_I^F and δ_{II}^F are the ultimate opening and tangential displacements, respectively.

The Mode I and Mode II energies released at failure are computed from:

$$G_I = \int_0^{\delta_I^{FM}} \sigma_{zz} d\delta_I \quad (16)$$

$$G_{II} = \int_0^{\delta_{II}^{FM}} \sqrt{\tau_{xz}^2 + \tau_{yz}^2} d\delta_{II}$$

where δ_I^F and δ_{II}^F are the Mode I and Mode II relative displacements at failure under mixed-mode loading. The ultimate opening displacement for any mixed-mode criterion can be calculated by substituting Eq. 16 into the appropriate interaction law. Using the definition of the mixed-mode relative displacement δ_m in Eq. 8 and the mode mixity ratio β given by Eq. 11, one can solve for the

ultimate relative displacement δ^F . For the power law given by Eq. 13, the ultimate relative displacement is found to be

$$\delta^F = \frac{2(1+\beta^2)}{K_p \delta_o} \left[\left(\frac{1}{G_{Ic}} \right)^\alpha + \left(\frac{\beta^2}{G_{IIc}} \right)^\alpha \right]^{-\frac{1}{\alpha}} \quad (17)$$

For the B-K criterion, the ultimate relative displacement is

$$\delta^F = \frac{2}{K_p \delta_o} \left[G_{Ic} + (G_{IIc} - G_{Ic}) \left(\frac{\beta^2}{1+\beta^2} \right)^\eta \right] \quad (18)$$

In summary, the mixed mode softening law presented above is a single-variable response similar to the bilinear single-mode law illustrated in Figure 4. Only one state variable, the relative displacement variable δ_m , is used to track the damage at the interface. By recording the highest value attained by δ_m , the unloading response is as shown in Figure 4. The displacements for initiation $\delta^0(\beta)$ and ultimate failure $\delta^F(\beta)$ are functions of the mode mixity

β . The relative displacement $\delta^0(\beta)$ is computed with Eq. 12, and $\delta^F(\beta)$ is computed with either Eq. 17 or Eq. 18.

The required material parameters are the penalty stiffness K_p , the interlaminar strengths T and S , the material toughnesses G_{Ic} and G_{IIc} and either η or α .

The ultimate relative displacements obtained from Eqs. 17 and 18 can be contrasted to the displacement obtained from the mixed mode criterion developed in previous work⁹. The criterion in Ref. 9 is based on a quadratic interaction between approximations to Eqs. 16, while Eqs. 17 and 18 are exact.

A mixed-mode softening law can be illustrated in a single 3D map by representing Mode I on the 2-3 plane, and Mode II in the 1-3 plane, as shown in Figure 6. The triangle $O-T-\delta_I^F$ is the bilinear material response in pure Mode I and $O-S-\delta_{II}^F$ is the bilinear material response in pure Mode II. It can be observed that the tensile strength T is lower than the shear strength S , and the ultimate displacement in shear is lower than in tension. In this three-dimensional map, any point on the 0-1-2 plane represents a mixed-mode relative displacement.

Under mixed mode, damage initiates at δ^0 , and complete fracture is reached at δ^F . Consequently, the tractions for Mode I and Mode II under mixed mode loading follow the reduced curves $O-T^M-\delta_I^{FM}$ and $O-S^M-\delta_{II}^{FM}$, respectively. The areas under these two curves represent the fracture energies under mixed mode represented by Eqs. 16.

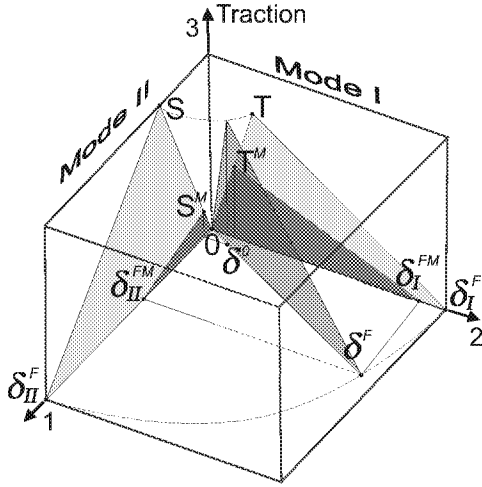


Figure 6. Combined plot of single-mode bilinear material responses.

The map of all softening responses under mixed mode is illustrated in Figure 7. The curve *FI* represents the tractions resulting from the displacements at the onset of damage given by Eq. 12, while the curve labeled *G* represents the ultimate relative displacements calculated with Eq. 17 or Eq. 18. The triangle *O-A-B* is the bilinear softening law for a mixed-mode relative displacement of δ_m . The triangle *O-A-B* is identical to the triangle 0-2-4 in Figure 4. For reference, the triangle 0-C-D in Figure 7 is the Mode I bilinear softening response. It can also be observed that the effect of compression on the material response is neglected.

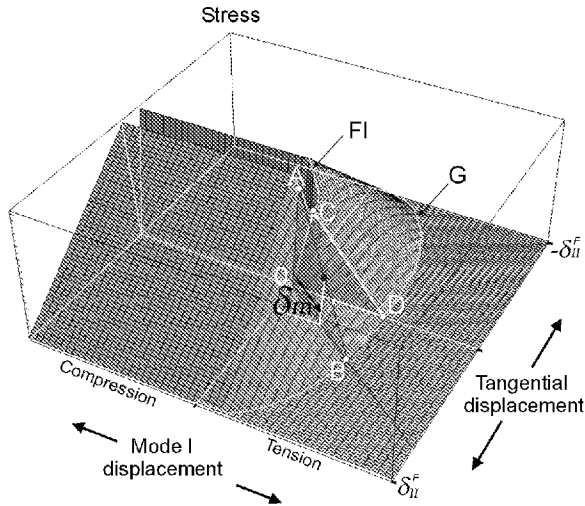


Figure 7. Map of strain softening response for mixed mode delamination.

Element Formulation

The element stiffness matrix is based on the standard isoparametric linear Lagrangian interpolation functions for

three-dimensional (8-node) elements. The relative displacements between the top and the bottom faces of the element in a local coordinate frame x - y - z are

$$\begin{Bmatrix} \delta_z \\ \delta_x \\ \delta_y \end{Bmatrix} = \begin{Bmatrix} w \\ u \\ v \end{Bmatrix}_{top} - \begin{Bmatrix} w \\ u \\ v \end{Bmatrix}_{bot} = \mathbf{B} \mathbf{U} \quad (19)$$

where \mathbf{B} is the matrix relating the element's degrees of freedom \mathbf{U} to the relative displacements between the top and bottom interfaces.

The three-dimensional form of Eq. 3 is

$$\boldsymbol{\sigma} = (\mathbf{I} - \mathbf{D}) \mathbf{C} \boldsymbol{\delta} \quad \text{or} \quad \begin{Bmatrix} \sigma_z \\ \tau_{xz} \\ \tau_{yz} \end{Bmatrix} = (\mathbf{I} - \mathbf{D}) \mathbf{C} \begin{Bmatrix} \delta_z \\ \delta_x \\ \delta_y \end{Bmatrix} \quad (20)$$

where \mathbf{I} is the identity matrix, \mathbf{C} is the undamaged constitutive matrix

$$\mathbf{C} = \begin{bmatrix} K_p & 0 & 0 \\ 0 & K_p & 0 \\ 0 & 0 & K_p \end{bmatrix} \quad (21)$$

and \mathbf{D} is a diagonal matrix representing the damage accumulated at the interface:

$$\mathbf{D} = \begin{bmatrix} d & 0 & 0 \\ 0 & d & 0 \\ 0 & 0 & d \end{bmatrix} \quad (22)$$

The term d on the diagonal is the damage parameter, which is a nonlinear function of δ_m^{\max} , the highest mixed-mode relative displacement experienced by the material

$$d = \frac{\delta^F (\delta_m^{\max} - \delta^0)}{\delta_m^{\max} (\delta^F - \delta^0)} \quad (23)$$

Using the maximum value of the relative displacement rather than the current value prevents healing of the interface. δ_m^{\max} is the only state variable that needs to be stored in the database to track the accumulation of damage.

The minimization of the potential energy subjected to the kinematic constraints of Eq. 19 leads to the usual integral over the area of the element, which gives the following element stiffness^{11, 21}:

$$\mathbf{K}_{elem} = \int_A \mathbf{B}^T ((\mathbf{I} - \mathbf{D}) \mathbf{C}) \mathbf{B} dA \quad (24)$$

The integration is performed numerically using a Newton-Cotes integration, which has been shown to perform better than Gaussian integration in problems involving strain softening^{15, 16}. The integration points of a zero-thickness decohesion element coincide with the four corners of the element. Since the material softening response is evaluated at each integration point, the element can soften one corner at a time, giving it the potential to model non self-similar delamination growth.

Nonlinear Solution

The nonlinear solution of the problems presented here was performed using standard ABAQUS procedures. However, the softening nature of the interface element constitutive equation causes convergence difficulties in the solution of the analysis. Schellekens¹⁶ recently suggested that in problems where failure is highly localized the displacement norm in Riks method should be determined considering only the dominant degrees of freedom. May²⁵ describes a new automated solution procedure for structures with strain-softening materials that is based on a constraint equation that uses only the displacement parameters associated with the localized failure zone in such structures. Unfortunately, a local arc-length procedure was not available for the analyses presented here.

Results and Discussion

Three test problems were selected to validate the decohesion elements. The first problem consists of the double cantilever beam (DCB) test used to determine Mode I toughness. The second problem modeled consists of the end-notched flexure test (ENF) used for Mode II toughness. The third test is the mixed bending mode test (MMB). All three of these problems have analytical solutions that were developed by Mi and Crisfield¹⁹. These closed form solutions provide an approximate framework against which to assess the FE models.

DCB Test for Mode I

The ASTM standard specimen used to determine the interlaminar fracture toughness in Mode I (G_{IC}) is the double-cantilever beam (DCB) specimen. This specimen is made of a unidirectional fiber-reinforced laminate containing a thin insert at the mid-plane near the loaded end. A 15-cm.-long specimen, 2 cm.-wide, and composed of two 1.98-mm-thick plies of unidirectional material was tested by Morais²⁶. The initial crack length is 5.5 cm. The properties of the graphite material are shown in Table 1, and the properties of the interface are shown in Table 2.

Table 1. Properties of the Graphite/Epoxy material²⁶.

E_{11}	$E_{22}=E_{33}$	$\nu_{12}=\nu_{13}$	ν_{23}	$G_{12}=G_{13}$	G_{23}
150. GPa	11. GPa	0.25	0.45	6.0 GPa	3.7 GPa

Table 2. Properties of the DCB specimen interface²⁶.

G_{Ic}	G_{IIc}	T	S	K_p
0.268 N/mm	1.45 N/mm	30. MPa	40. MPa	10^6 N/mm ³

Using Eqs. 9 and the properties of the interface shown in Table 2, the relative Mode I and Mode II displacements for damage onset are $\delta_I^0 = 30. \times 10^{-6}$ mm. and $\delta_{II}^0 = 40. \times 10^{-6}$ mm., respectively. The corresponding ultimate relative displacements calculated from Eqs. 15 are $\delta_I^F = 17.9 \times 10^{-3}$ mm. and $\delta_{II}^F = 72.5 \times 10^{-3}$ mm.

The ABAQUS finite element model, which is shown deformed in Figure 8, consists of two layers of C3D8I incompatible-mode 8-noded elements. C3D8I elements are superior in bending to other low-order continuum elements. The anticlastic effects were neglected and only one element was used across the width. One hundred and twenty elements were used along the span of the model shown in Figure 8.

A plot of reaction force as a function of the applied end displacement d is shown in Figure 9. The beam solution was developed by Mi and Crisfield¹⁹ for isotropic adherend materials and using plane stress assumptions. Note that the beam solution is somewhat stiffer than the test and FEM results which is probably due to the assumption of isotropy in the analytical solution. After the initiation of delamination, fiber bridging in the test specimen causes a small drift in the response compared to the FEM and analytical solutions.

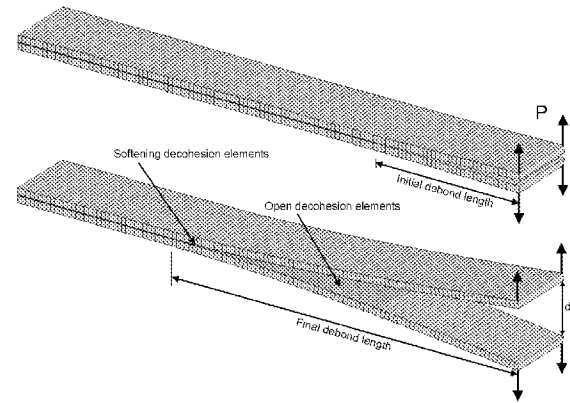


Figure 8. Model of DCB test specimen.

Numerical studies with different element sizes indicate that the accuracy of the prediction can be significantly lower if the size of the elements used in the softening zone

is greater than some maximum value. The maximum predicted load sustained by the DCB specimen calculated using several mesh densities is shown in Figure 10. The results indicate that poor results are obtained for this problem when the element size is greater than 1.25 mm. This mesh size is consistent with the results of Gonçalves¹⁰, who used 1-mm.-long 18-node quadratic elements for the analysis of a DCB specimen.

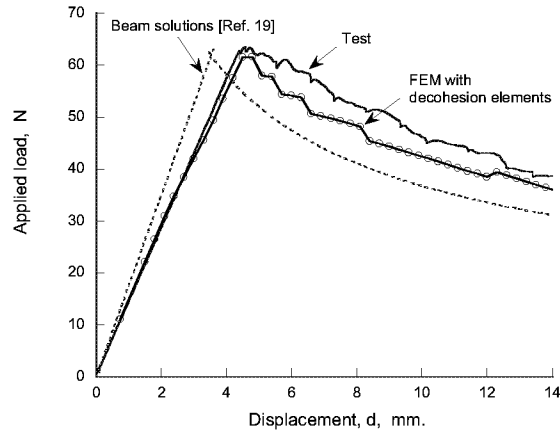


Figure 9. Load-deflection response of DCB test.

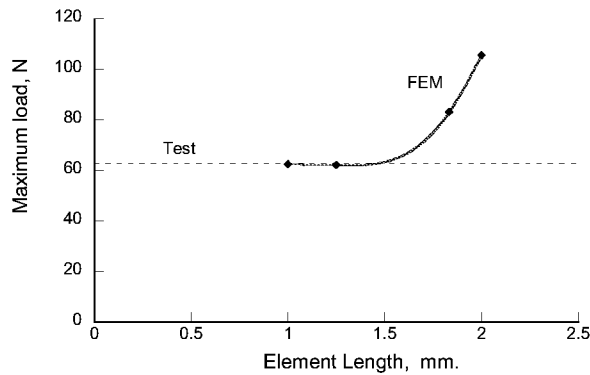


Figure 10. Debond load as a function of element size.

ENF Test for Mode II

Even though the end-notched flexure test specimen shown in Figure 11 exhibits unstable crack propagation for short crack lengths, its simplicity makes it a common test to measure Mode II fracture toughness. The length of the specimen modeled here is 10 cm., its width is 1 cm., and the initial debond length is 3 cm. Aluminum adherends were used rather than composite to achieve a closer approximation to the analytical solutions calculated by Mi¹⁹. The thickness of the adherends is 1.5 mm. The properties of the interface are the same as for the DCB model.

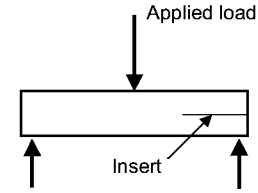


Figure 11. ENF test specimen.

The load-deflection responses for the finite element model and the analytical prediction are shown in Figure 12. It can be observed that both solutions are in excellent agreement.

Mixed Mode Bending Test

The most widely used specimen for mixed-mode fracture is the mixed-mode bending (MMB) specimen shown in Figure 13, which was proposed by Reeder and Crews²⁷ and later re-designed to minimize geometric nonlinearities²⁸. The main advantages of the MMB test method are the possibility of using virtually the same specimen configuration as for Mode I tests and varying the mixed mode ratio from pure Mode I to pure Mode II.

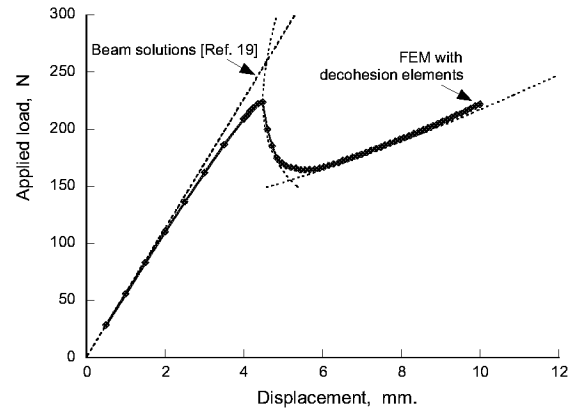


Figure 12. Analytical and FEM load-deflection curves for ENF test.

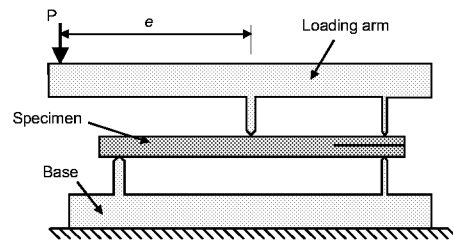


Figure 13. MMB test specimen.

The specimen analyzed here has a length of 10 cm., a width of 1 cm., and an initial debond length of 3 cm. The thickness of the aluminum adherends is 1.5 mm. The

properties of the interface are the same for the DCB and ENF models. The length of the MMB lever e was chosen as 43.72mm, which corresponds to a ratio of 1 for G_I/G_{II} and to a ratio of 2.14 between the load at the mid-span of the beam and the opening load. The MMB load fixture is simulated by applying an opening load of 100 N. at the edge of the debond, and an opposite load of 214 N. at the mid-span of the beam.

The model is composed of two layers of 100 C3D8I solid elements. A deformed plot of the finite element model is shown in Figure 14.

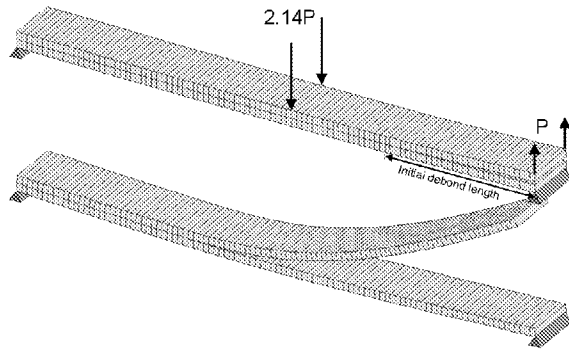


Figure 14. Deformed plot of MMB Model.

The load deflection curve calculated from FEM and analytical constant-G curves derived using the beam solutions in Ref. 19 are shown in Figure 15 for linear interaction between the energy release rates ($\alpha=1$), quadratic interaction ($\alpha=2$), and for a 3-parameter fit using $\eta=1.45$. In addition, the results of the mixed mode criterion from Ref. 9 are also represented. No test results were available for the configuration analyzed. However, the FEM results compare well with their corresponding analytical curves. The FEM results with $\eta=1.45$ are based on a fit of mixed-mode test data, so they represent the most accurate solution and a significant improvement over the criterion developed in Ref. 9.

Concluding Remarks

A new criterion for the simulation of progressive delamination using decohesion elements was presented. Decoherence elements are placed between layers of solid elements and they open in response to the loading situation. The onset of damage and the growth of delamination can be simulated without previous knowledge about the location, the size, and the direction of propagation of the delaminations. A softening law for mixed-mode delamination that can be applied to any interaction law was proposed. The criterion uses a single state variable, the maximum relative displacement δ_m^{\max} , to track the damage at the interface under general loading conditions. For the linear and quadratic criteria, the material properties

required to define the element constitutive equation are the interlaminar fracture toughnesses and the corresponding strengths. The B-K interaction law requires additionally a material parameter η that is determined from standard mixed-mode tests.

Three examples were presented that test the accuracy of the method. Simulations of the DCB and ENF test represent cases of single-mode delamination. The MMB test that was simulated has equal Mode I and Mode II loading conditions. The examples analyzed indicate that the mixed-mode criteria can predict the strength of composite structures that exhibit progressive delamination.

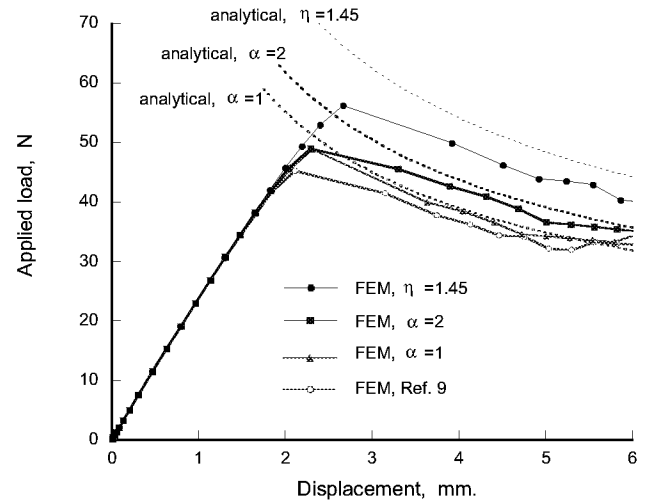


Figure 15. Predicted load-deflection plots for MMB test.

References

- 1) Dávila, C.G., and Johnson, E.R., "Analysis of Delamination Initiation in Postbuckled Dropped-Ply Laminates," AIAA Journal, April 1993.
- 2) Camanho, P.P., and Matthews, F.L., "Delamination Onset Prediction in Mechanically Fastened Joints in Composite Laminates," Journal of Composite Materials, Vol. 33, No. 10, 1999, pp. 906-927.
- 3) Rybicki, E.F., and Kanninen, M.F., "A Finite Element Calculation of Stress Intensity Factors by a Modified Crack Closure Integral," Engineering Fracture Mechanics, Vol. 9, 1977, pp. 931-939.
- 4) Camanho, P.P., Dávila, C.G., and Ambur, D.R., "Numerical Simulation of Delamination Growth in Composite Materials," NASA TP, NASA-TP-2001-211041, Hampton, VA, August 2001.
- 5) Barenblatt, G.I., "Mathematical Theory of Equilibrium Cracks in Brittle Failure," Advances in Applied Mechanics, Vol. 7, 1962.

- 6) Hilleborg, A., Modeer, M., and Petersson, P.E., "Analysis of Crack Formation and Crack Growth in Concrete by Fracture Mechanics and Finite Elements," *Cement and Concrete Research*, Vol. 6, 1976, pp. 773-782.
- 7) Needleman, A., "A Continuum Model for Void Nucleation by Inclusion Debonding," *Journal of Applied Mechanics*, Vol. 54, 1987, pp. 525-531.
- 8) Dávila, C.G., Camanho, P.P., and de Moura, M.F.S.F., "Progressive Damage Analyses of Skin/Stringer Debonding," *Proceedings of the American Society for Composites*, Blacksburg, VA, September 11, 2001.
- 9) Dávila, C.G., Camanho, P.P., and de Moura, M.F.S.F., "Mixed-Mode Decohesion Elements for Analyses of Progressive Delamination," *Proceedings of the 42nd AIAA/ASME/ASCE/AHS/ASC Structures, Structural Dynamics and Materials Conference*, Seattle, Washington, April 16-19, 2001.
- 10) Gonçalves, J.P.M., de Moura, M.F.S.F., de Castro, P.M.S.T., and Marques, A.T., "Interface Element Including Point-to-Surface Constraints for Three-Dimensional Problems with Damage Propagation," *Engineering Computations*, Vol. 17, No. 1, 2000, pp. 28-47.
- 11) de Moura, M.F.S.F., Gonçalves, J.P.M., Marques, A.T., and de Castro, P.M.S.T., "Modeling Compression Failure after Low Velocity Impact on Laminated Composites Using Interface Elements," *Journal of Composite Materials*, Vol. 31, 1997, pp. 1462-1479.
- 12) Petrossian, Z., and Wisnom, M.R., "Prediction of Delamination Initiation and Growth from Discontinuous Plies Using Interface Elements," *Composites Part A: Applied Science and Manufacturing*, Vol. 29, No. 5-6, 1998, pp. 503-515.
- 13) Reddy, J.N., Mello, F.J., and Guess, T.R., "Modeling the Initiation and Growth of Delaminations in Composite Structures," *Journal of Composite Materials*, Vol. 31, 1997, pp. 812-831.
- 14) Rice, J.R., "A Path Independent Integral and the Approximate Analysis of Strain Concentration by Notches and Cracks," *Journal of Applied Mechanics*, 1968, pp. 379-386.
- 15) Schellekens, J.C.J., and de Borst, R., "Numerical Simulation of Free Edge Delamination in Graphite-Epoxy Laminates under Uniaxial Tension," *Proceedings of the 6th International Conference on Composite Structures*, 1991, pp. 647-657.
- 16) Schellekens, J.C.J., and de Borst, R., "On the Numerical Integration of Interface Elements," *International Journal for Numerical Methods in Engineering*, Vol. 36, 1993, pp. 43-66.
- 17) Chen, J., Crisfield, M.A., Kinloch, A.J., Busso, E.P., Matthews, F.L., and Qiu, Y., "Predicting Progressive Delamination of Composite Material Specimens Via Interface Elements," *Mechanics of Composite Materials and Structures*, Vol. 6, 1999, pp. 301-317.
- 18) Mi, Y., Crisfield, M.A., Davies, G.A.O., and B., H.H., "Progressive Delamination Using Interface Elements," *Journal of Composite Materials*, Vol. 32, 1998, pp. 1246-1273.
- 19) Mi, Y., and Crisfield, M.A., "Analytical Derivation of Load/Displacement Relationships for Mixed-Mode Delamination and Comparison with Finite Element Results," *Imperial College, Department of Aeronautics*, London, 1996.
- 20) Daudeville, L., Allix, O., and Ladevèze, P., "Delamination Analysis by Damage Mechanics: Some Applications," *Composites Engineering*, Vol. 5, No. 1, 1995, pp. 17-24.
- 21) de Moura, M.F.S.F., Gonçalves, J.P.M., Marques, A.T., and de Castro, P.M.S.T., "Prediction of Compressive Strength of Carbon-Epoxy Laminates Containing Delamination by Using a Mixed-Mode Damage Model," *Composite Structures*, Vol. 50, 2000, pp. 151-157.
- 22) Reeder, J.R., "An Evaluation of Mixed-Mode Delamination Failure Criteria," *NASA TM 104210*, Hampton, VA, 1992.
- 23) Benzeggagh, M.L., and Kenane, M., "Measurement of Mixed-Mode Delamination Fracture Toughness of Unidirectional Glass/Epoxy Composites with Mixed-Mode Bending Apparatus," *Composites Science and Technology*, Vol. 56, No. 4, 1996, pp. 439-449.
- 24) Reeder, J.R., "Refinements to the Mixed-Mode Bending Test for Delamination Toughness," *Proceedings of the 14th ASTM Symposium on Composite Materials: Testing and Design*, Pittsburgh, PA, to be presented March 2002.
- 25) May, I.M., and Duan, Y., "A Local Arc-Length Procedure for Strain Softening," *Computers & Structures*, Vol. 64, No. 1-4, 1997, pp. 297-303.
- 26) Morais, A.B., Marques, A.T., and de Castro, P.T., "Estudo Da Aplicação de Ensaios de Fractura Interlaminar de Modo I a Laminados Compósitos Multidireccionais," *Proceedings of the 7as Jornadas De Fractura, Sociedade Portuguesa de Materiais*, Portugal, 2000, pp. 90-95.
- 27) Crews, J.H., and Reeder, J.R., "A Mixed-Mode Bending Apparatus for Delamination Testing," *NASA TM 100662*, Hampton, VA, 1988.
- 28) Reeder, J.R., and Crews, J.H., "Nonlinear Analysis and Redesign of the Mixed-Mode Bending Delamination Test," *NASA TM-102777*, Hampton, VA, 1991.